REPORT DOCUMENTATION PAGE

Form Approved OMB No. 0704-0188

1. REPORT DATE *(DD-MM-YYYY)*
04-01-2006

REPRINT

4. TITLE AND SUBTITLE
QUANTUM LATTICE REPRESENTATION OF 1D MHD TURBULENCE WITH ARBITRARY TRANSPORT COEFFICIENTS

5a. CONTRACT NUMBER

5b. GRANT NUMBER

5c. PROGRAM ELEMENT NUMBER
61102F

6. AUTHOR(S)
J. Yepez, G. Vahala* and L. Vahala

5d. PROJECT NUMBER
2304

5e. TASK NUMBER
0T

5f. WORK UNIT NUMBER
B1

7. PERFORMING ORGANIZATION NAME(S) AND ADDRESS(ES)
Air Force Research Laboratory/VSBYA
29 Randolph Road
Hanscom AFB MA 01731-3010

8. PERFORMING ORGANIZATION REPORT NUMBER
AFRL-VS-HA-TR-2005-1199

9. SPONSORING / MONITORING AGENCY NAME(S) AND ADDRESS(ES)

10. SPONSOR/MONITOR'S ACRONYM(S)

11. SPONSOR/MONITOR'S REPORT NUMBER(S)

12. DISTRIBUTION / AVAILABILITY STATEMENT
Approved for Public Release; Distribution Unlimited.

*Dept Physics, College of William & Mary, Williamsburg, VA
**Dept Electrical & Comp Engr, Old Dominion University, Norfolk, VA

13. SUPPLEMENTARY NOTES
REPRINTED FROM: Quantum Information and Computation III, edited by E.J. Donkor, A.R. Pirich, H.E. Brandt, PROCEEDINGS OF SPIE, Vol 5815(SPIE, Bellingham, WA 2005)doi:10.1117/12.603029.

14. ABSTRACT

The quantum Boltzmann equation method is demonstrated by numerically predicting the time-dependent solutions of the velocity and magnetic fields governed by nonintegrable magnetohydrodynamic equations in one spatial dimension. The method allows arbitrary tuning of the value of the viscosity and resistivity transport coefficients without compromising numerical integrity even near the zero dissipation and turbulent regime where shock front discontinuities emerge.

15. SUBJECT TERM:
Quantum computing Quantum Boltzmann equation
Magnetohydrodynamic turbulence

16. SECURITY CLASSIFICATION OF:			**17. LIMITATION OF ABSTRACT**	**18. NUMBER OF PAGES**	**19a. NAME OF RESPONSIBLE PERSON**
a. REPORT UNCLAS	UNCLAS	**c. THIS PAGE** UNCLAS	SAR		Jeffrey Yepez
					19b. TELEPHONE NUMBER *(include area code)* 781-377-5957

Quantum lattice representation of 1D MHD turbulence with arbitrary transport coefficients

Jeffrey Yepez[a] and George Vahala[b] and Linda Vahala[c]

[a]Air Force Research Laboratory, 29 Randolph Road, Hanscom Field, Massachusetts 01731;
[b]Department of Physics, College of William & Mary, Williamsburg, VA 23187;
[c]Department of Electrical & Comp. Engineering, Old Dominion University, Norfolk, VA 23529

ABSTRACT

The quantum Boltzmann equation method is demonstrated by numerically predicting the time-dependent solutions of the velocity and magnetic fields governed by nonintegrable magnetohydrodynamic equations in one spatial dimension. The method allows arbitrary tuning of the value of the viscosity and resistivity transport coefficients without compromising numerical integrity even near the zero dissipation and turbulent regime where shock front discontinuities emerge.

Keywords: quantum computing, quantum Boltzmann equation, magnetohydrodynamic turbulence

1. INTRODUCTION

Parallel quantum algorithms[1] have been developed to numerically predict time-dependent field solutions of the diffusion equation,[2] the nonlinear Burgers equation,[3,4] the one dimensional equations for magnetohydrodynamic turbulence,[5] the Korteweg de Vries equation,[6] the nonlinear Schroedinger equation,[6,7] and the Manakov equations.[8,9] The first parallel quantum algorithms for the diffusion and Burgers equations have with success been experimentally tested on quantum information processing prototypes of parallel quantum computers (or type-II quantum computers[10]) using spatial nuclear magnetic resonance spectroscopy on a linear array (in space and in reciprocal space) of segmented ensembles of two-qubit labeled chloroform molecules.[11–13]

Here, we generalize our parallel quantum algorithm for modeling magnetohydrodynamic (MHD) turbulence. This algorithm is based upon the quantum algorithms for the diffusion[2] and Burgers equations[3,4]; it can be implemented on a parallel quantum computer with pairs of labeled chloroform molecules. The intent of this paper is solely to demonstrate the quantum Boltzmann equation method, so all the details about the microscopic quantum mechanical implementation of the method have been replaced with a friendlier mesoscopic treatment. The quantum mechanical foundation of the method lends it several advantageous features as a tool for computational physics. First, there is inherent numerical stability. Second, there is a corresponding entropy function description of the model dynamics and an entropy theorem, although for economy and brevity the details of the entropy function are not presented here. The Boltzmann collision function can be computed directly without the need of root finding as is required for entropic lattice Boltzmann equation models of turbulence.[14–16] Although the quantum algorithm presented here was originally developed for a parallel quantum computing architecture, the quantum Boltzmann equation is a practical algorithmic method for presentday classical computers.

Turbulence is plagued by spatiotemporal intermittency involving coherent structures – structures that are at odds with the simple scale-similarity arguments. Insight into these coherent structures comes by examining

Further author information: (Send correspondence to J.Y)
E-mail: jeffrey.yepez@hanscom.af.mil
Telephone: 1 781 377 5957
World wide web: http://qubit.plh.af.mil

Quantum Information and Computation III, edited by Eric J. Donkor, Andrew R. Pirich, Howard E. Brandt, Proceedings of SPIE Vol. 5815 (SPIE, Bellingham, WA, 2005)
0277-786X/05/$15 · doi: 10.1117/12.603029

simplified models and the simplest model exhibiting Alfvenization (the exchange of fluid and magnetic energies) are the 1D equations[17,18]

$$\frac{\partial v}{\partial t} + v\frac{\partial v}{\partial x} = -\frac{\partial}{\partial x}\left(\frac{B^2}{2}\right) + \mu\frac{\partial^2 v}{\partial x^2} \tag{1}$$

$$\frac{\partial B}{\partial t} + \frac{\partial}{\partial x}(vB) = \eta\frac{\partial^2 B}{\partial x^2} \tag{2}$$

for the velocity field $\vec{v} = v(x)\hat{x}$ and the magnetic field $\vec{B} = B(x)\hat{z}$. The transport coefficient μ is the fluid viscosity and η is the plasma resistivity. These 1D equations are derived from the full MHD equations when the fluid density length scales are much longer than those of the B field.[17,18] To leading order, this results in a constant density so that (1) forms a closed set of equations for v and B. Adding a y-component of the magnetic field gives a 1D model for solar flares.[19] In Elsasser variables $z_\pm = v \pm B$, (1) can be written in symmetric form

$$\frac{\partial z_\pm}{\partial t} + z_\pm\frac{\partial z_\pm}{\partial x} = \mu\frac{\partial^2 z_\pm}{\partial x^2} \pm \frac{1}{2}(\eta - \mu)\frac{\partial^2 (z_+ - z_-)}{\partial x^2}. \tag{3}$$

If the transport coefficients are equal, $\eta = \mu$, then (3) reduces to two uncoupled nonlinear Burgers equations for $z_\pm$. [In the limit $B \equiv 0$, (1) reduces to Burgers equation for v]. The Burgers equation[20] is a well-known paradigm for Navier-Stokes turbulence and has also been studied extensively for many decades as a simplified model for boundary layer behavior, shock wave formation, mass transport, self-organized criticality and growing interfaces. It is also a test-bed for numerical methods since a general analytic solution exists.[21,22] In Burgers turbulence, regions where $\frac{\partial v}{\partial x} < 0$ steepen into shock singularities, while regions where $\frac{\partial v}{\partial x} > 0$ become smoother. However, with the inclusion of the B field, there is now a magnetic back-pressure in (1) that is absent from Burgers equation. In particular, the B field will concentrate in regions of the velocity shock, softening the shock front. For $\eta \neq \mu$, (1) is non-integrable.

To model (1) we use two quantum Boltzmann equations in a two step algorithm for an ordered one dimensional array of L number of nodes, enumerated by a "spatial" integer coordinate $x = 1, 2, ..., L$. At each node are four probability values $0 \leq p_a \leq 1$, for $a = 1, 2, 3, 4$ and they are called *occupation probabilities*. The first step of the algorithm encodes the $B(x)$ field using the probability fields $p_3(x)$ and $p_4(x)$:

$$p_3(x) = \frac{B(x)}{2} \qquad p_4(x) = \frac{B(x)}{2} \tag{4}$$

The second step uses the following quantum Boltzmann equation to update these two probability fields:

$$p_3'(x-1) = p_3(x) - [p_3(x) - p_4(x)]\sin^2\beta \tag{5}$$

$$p_4'(x+1) = p_4(x) + [p_3(x) - p_4(x)]\sin^2\beta. \tag{6}$$

The third step assigns the new values to the $B(x)$ field:

$$B(x) = p_3'(x) + p_4'(x). \tag{7}$$

The fourth step encodes the $v(x)$ and $B(x)$ fields using all four probability fields:

$$p_{1,2}(x) = \frac{1}{2}[1 + v(x) \pm B(x)] = p_{3,4}(x). \tag{8}$$

(Only on the first pass through the algorithm, to initialize it in local equilibrium, we use the encoding:

$$p_1(x) = d_1[\cot\theta, 1 + v(x) + B(x)] \tag{9}$$

$$p_2(x) = d_2[\cot\theta, 1 + v(x) - B(x)] \tag{10}$$

$$p_3(x) = d_1[\cot\theta, 1 + v(x) + B(x)] \tag{11}$$

$$p_4(x) = d_2[\cot\theta, 1 + v(x) - B(x)], \tag{12}$$

where the local equilibrium functions

$$d_1(\alpha,\rho) = \frac{\rho}{2} + \frac{1}{2\alpha}\left[\sqrt{1+\alpha^2} - \sqrt{1+\alpha^2(\rho-1)^2}\right] \quad (13)$$

$$d_2(\alpha,\rho) = \frac{\rho}{2} - \frac{1}{2\alpha}\left[\sqrt{1+\alpha^2} - \sqrt{1+\alpha^2(\rho-1)^2}\right] \quad (14)$$

are the zeros of the quantum collision function.) The fifth step uses the following quantum Boltzmann equation to update all the probability fields:

$$p_1'(x-1) = p_1(x) - [p_1(x) - p_2(x)]\sin\theta + \sqrt{p_1(x)[1-p_1(x)]p_2(x)[1-p_2(x)]}\sin 2\theta \quad (15)$$

$$p_2'(x+1) = p_2(x) + [p_1(x) - p_2(x)]\sin\theta - \sqrt{p_1(x)[1-p_1(x)]p_2(x)[1-p_2(x)]}\sin 2\theta \quad (16)$$

$$p_3'(x-1) = p_3(x) - [p_3(x) - p_4(x)]\sin\theta + \sqrt{p_3(x)[1-p_3(x)]p_4(x)[1-p_4(x)]}\sin 2\theta \quad (17)$$

$$p_4'(x+1) = p_4(x) + [p_3(x) - p_4(x)]\sin\theta - \sqrt{p_3(x)[1-p_3(x)]p_4(x)[1-p_4(x)]}\sin 2\theta \quad (18)$$

The final step uses an inverse of (8) to compute the updated values of the $v(x)$ and $B(x)$ fields from the new occupations probabilities by the following assignments:

$$v'(x) = \frac{1}{2}[p_1(x) + p_2(x) + p_3(x) + p_4(x)] - 1 \quad (19)$$

$$B'(x) = \frac{1}{2}[p_1(x) + p_2(x) - p_3(x) - p_4(x)]\,. \quad (20)$$

At this point, one iteration of the algorithm is completed and time is advanced by one unit Δt. In this way, a time history of the v and B fields can be generated by looping through the enumerated steps.

2. EFFECTIVE FIELD THEORY

After some algebra for the special case where $\beta = 0$ and $\theta = \frac{\pi}{4}$, and with the encoding (8) and the asignment (1) formulae, it follows that the mesoscopic transport equation (1) can be written directly as a finite difference equation in the $v(x)$ and $B(x)$ fields:

$$v'(x) = \frac{1}{2}[v(x-1) + v(x+1)] + \frac{1}{4}\left[v(x-1)^2 - v(x+1)^2\right] + \frac{1}{4}\left[B(x-1)^2 - B(x+1)^2\right] \quad (21)$$

$$B'(x) = \frac{1}{2}[B(x+1) + B(x-1)] + \frac{1}{2}\left[v(x-1)B(x-1) - v(x+1)B(x+1)\right]. \quad (22)$$

A more general set of finite difference equations than (2) can be predicted by the quantum Boltzmann equation method for arbitrary θ, but are too lengthy to include here *.

The macroscopic scale effective field theory for $v(x,t)$ and $B(x,t)$ follows from taking the continuum limit of (2) with the ordering $\Delta x \sim \mathcal{O}(\varepsilon)$ and $\Delta t \sim \mathcal{O}(\varepsilon^2)$. We obtain (in lattice units $\Delta x = 1 = \Delta t$)

$$\frac{\partial v}{\partial t} + v\frac{\partial v}{\partial x} = \frac{1}{2}\frac{\partial^2 v}{\partial x^2} - B\frac{\partial B}{\partial x} + \mathcal{O}(\varepsilon^3) \quad (23)$$

$$\frac{\partial B}{\partial t} + v\frac{\partial B}{\partial x} = \frac{1}{2}\frac{\partial^2 B}{\partial x^2} - B\frac{\partial v}{\partial x} + \mathcal{O}(\varepsilon^3). \quad (24)$$

This is just the 1D MHD (1) in the special case where the kinematic shear viscosity and resistivity transport coefficients are equal, $\mu = \eta = \frac{\Delta x^2}{2\Delta t}$. If we make an Elsasser variables substitution, $z_\pm = v \pm B$, then (23) and (24) simplify into two uncoupled nonlinear Burgers equations for $z_\pm$, see (3). We now proceed from the integrable 1D MHD with $\mu = \eta$ to the non-integrable case of unequal transport coefficients, $\mu \neq \eta$.

*The unitary collision operators are implemented with perfect control and the occupation probabilities are measured exactly. These assumptions hold only for an ideal experimental setup. We address actual quantum control and Von Neuman projective shot noise in our papers on experimental parallel quantum computing with NMR.[11–13]

After some algebra for the special case where $\beta = \frac{\pi}{4}$ and $\theta = \frac{\pi}{4}$, and with the encoding formulae (4) and the mesoscopic transport equation (1) and the asignment formula(7), and then also with the encoding formulae (8) and the quantum Boltzmann equation (1) and the asignment formulae (1), it follows that the dynamics of the $v(x)$ and $B(x)$ fields can be written directly as a finite difference equation:

$$v'(x) = \frac{1}{2}\left[v(x-1)+v(x+1)\right] + \frac{1}{4}\left[v(x-1)^2 - v(x+1)^2\right] + \frac{1}{16}\left[B(x-2)-B(x+2)\right]\left[B(x-1)+2B(x)+B(x+1)\right] \quad (25)$$

$$B'(x) = \frac{1}{4}\left[B(x-2)+2B(x)+B(x+2)\right] + \frac{1}{4}\left[v(x-1)B(x-2) + \left[v(x-1)-v(x+1)\right]B(x) - v(x+1)B(x+2)\right]. \quad (26)$$

Again proceeding to the continuum limit by Taylor expanding (2), we obtain our desired 1D MHD equations with unequal transport coefficients: viscosity $\mu = \frac{\Delta x^2}{2\Delta t}$ and resisitivity $\eta = \frac{\Delta x^2}{\Delta t}$. In the general case where $\frac{\pi}{4} \leq \theta < \frac{\pi}{2}$ and $\frac{\pi}{4} \leq \beta < \frac{\pi}{2}$, we obtain the following effective field theory:

$$\frac{\partial v}{\partial t} + v\frac{\partial v}{\partial x} = \mu\frac{\partial^2 v}{\partial x^2} - B\frac{\partial B}{\partial x} + \mathcal{O}(\varepsilon^3) \quad (27)$$

$$\frac{\partial B}{\partial t} + v\frac{\partial B}{\partial x} = \eta\frac{\partial^2 B}{\partial x^2} - B\frac{\partial v}{\partial x} + \mathcal{O}(\varepsilon^3), \quad (28)$$

with adjustable transport coefficients for the viscosity and resistivity [†]:

$$\mu = \cot^2\theta\frac{\Delta x^2}{\Delta t} \qquad \eta = \left(\cot^2\theta + \cot^2\beta\right)\frac{\Delta x^2}{\Delta t}. \quad (29)$$

3. NUMERICAL TESTS

The 1D MHD equations are solved using the quantum Boltzmann equation method described above for initial profiles $v(x,0) = \cos\left(\frac{2\pi}{L}\right)$ and $B(x,0) = 0.1$ on a $L = 256\Delta x$ grid. The evolution of the fields are shown in Fig. 1 (low dissipation regime) and Fig. 2 (high dissipation regime). Regions of $\frac{\partial v}{\partial x} < 0$ steepen towards shocks while regions of $\frac{\partial v}{\partial x} > 0$ smooth. At first the B field rapidly increases by a factor of 10 and concentrates where velocity shocks form. Asymptotically in time (but when the nonlinear terms are important and before the profile linearly diffuses away) the velocity profile bifurcates and eventually becomes linear in x except at the shocks. There is a surprising cancellation of errors. If you look at the profiles of the occupation probabilities in Fig. 1 (low dissipation regime), they separately each have Gibbs oscillations. However, when the two occupation probability fields are added together forming the $v(x)$ field or subtracted forming the $B(x)$ field, the oscillations substantially cancel out because the oscillations are out of phase. The Gibbs oscillations subside altogether with higher grid resolution since its source is an under resolved shock front.

The B field asymptotically tends to a constant with spatial jumps around the velocity shock fronts. The linear sloped v field decays in time as does the constant B field. Indeed, we can check our model in this asymptotic region. Assuming $v(x,t) \longrightarrow a(t)x + b(t)$ and $B(x,t) \longrightarrow B(t)$, except at isolated locations corresponding to shock fronts, (1) yield constraint equations for $a(t)$, $c(t)$, and $B(t)$:

$$\frac{da}{dt} + a^2 = 0 \qquad \frac{db}{dt} + ab = 0 \qquad \frac{dB}{dt} + aB = 0. \quad (30)$$

The analytical solution of (30) yield asymptotic v and B field profiles

$$v(x,t) = \frac{x+k_2}{t+k_1} \qquad B(t) = \frac{k_3}{t+k_1}, \quad (31)$$

[†](29) based on previous results from modeling the Burgers equation, but their exact form has not yet been confirmed.

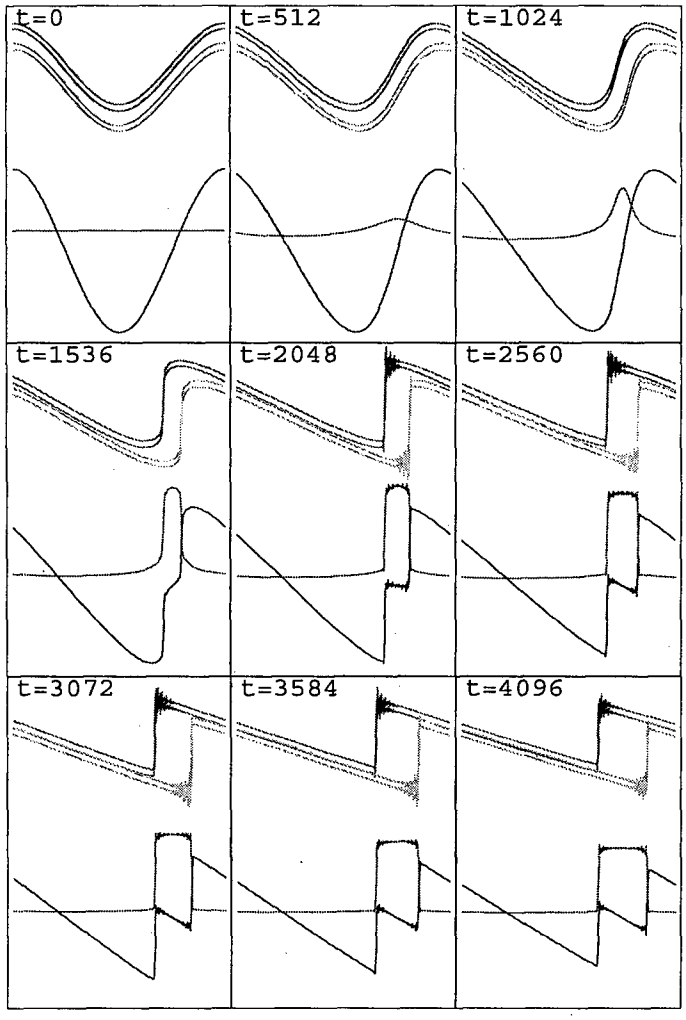

Figure 1. Simulation results in the low dissipation regime $\beta = 0$ and $\theta = 1.5$ radians. The blue curve is the velocity field. The red curve is the magnetic field. The purple curves are the first and second occupation probability fields (p_1 and p_2). The green curves are the third and fourth occupation probability fields (p_3 and p_4). There are four black curves; these are analytical predictions, based on the computed macroscopic field profiles, of the equilibrium occupation probabilities and they are in excellent agreement with the numerical predictions. The mesoscopic fields remain in local equilibrium. The simulation was carried out on a lattice with 256 nodes. Snapshots are shown at every 512 time steps. In regions of $\frac{\partial v}{\partial x} < 0$, shocks tend to form in the v-field with localized enhancement of the B-field. Asymptotically, v attains a constant slope with shock discontinuities while the B field is constant with discontinuities at the leading edges of the front. The extent of the Gibbs oscillations at the shock front is greater at the mesoscopic than at the macroscopic scale because of a fortuitous cancellation of errors.

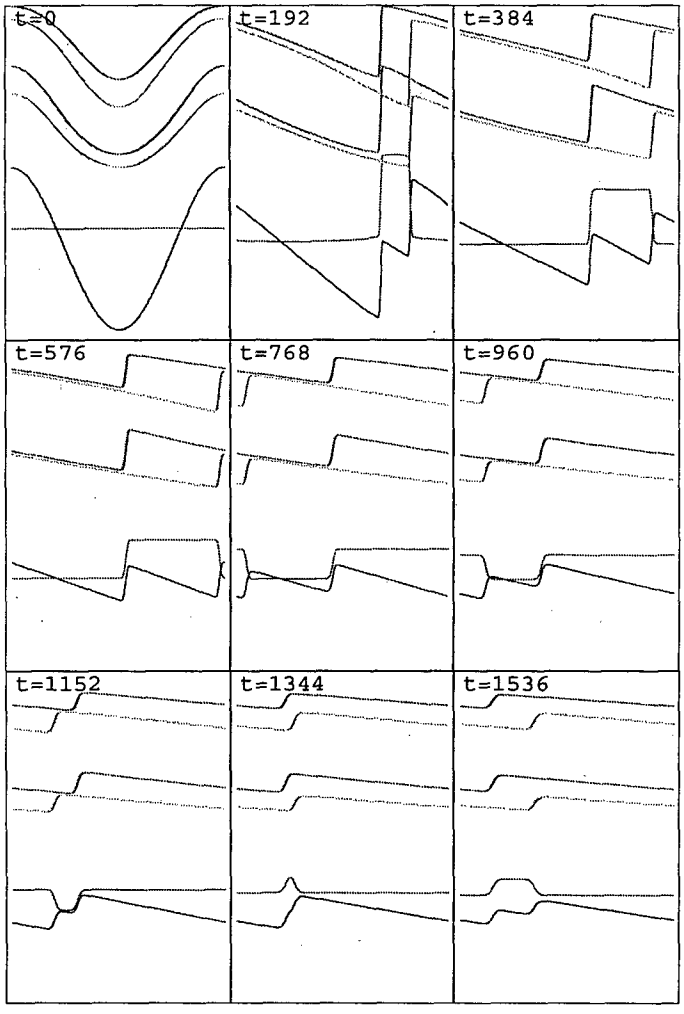

Figure 2. Simulation results in the high dissipation regime $\beta = 0$ and $\theta = \frac{\pi}{4}$, but otherwise similar to the previous figure (see Fig. 1 caption). No Gibbs oscillations occur since the shock front is spatially resolved.

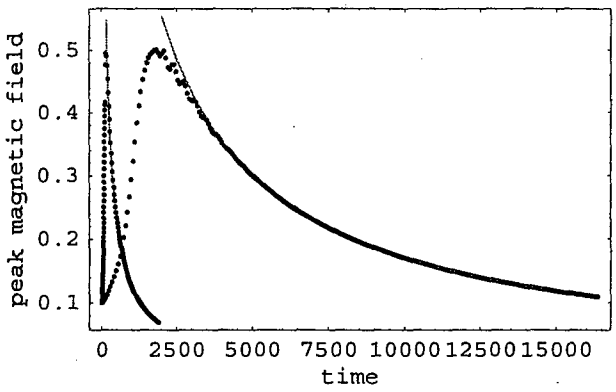

Figure 3. The time evolution of the B field at location $x = 192$ determined from the quantum algorithm (dotted curve). Two cases are shown. For the $\theta = \frac{\pi}{4}$ case, after the shock formation around $t \sim 200\Delta t$. For the $\theta = 1.5$ radians case, shock formation occurs latter in time at around $t \sim 2500\Delta t$. The analytical asymptotic solutions (red curves) shows the B field decays like t^{-1} as expected, see (31). There is excellent agreement between theory and the numerical solution over the whole dissipative regime from high to low resistivity.

with constants of integration k_1, k_2 and k_3. From the quantum simulations shown in Figs. 1 and 2, we plotted in Fig. 3 the B field at $x = 192$ as a time series (black dots). The solid curve is the asymptotic decay (31) derived from (1). The decay is fast for the high resistivity case and it is slow for the low resistivity case. There is excellent agreement after the shock has fully formed with the analytical asymptotic solutions (red curves) validating our model for 1D MHD with unequal and arbitrary transport coefficients.

4. FINAL REMARKS

The numerical simulation results plotted in Figs. 1 and 2 manifest a characteristic property of a type-II quantum algorithm. The expected value of the occupancy of the ground state and excited state of a microscopic qubit contained within a quantum mechanical node of the lattice (in the 1D MHD model presented here there would be four qubits per node) are shifted. The expectation value of the excited state is plotted in the purple and green curves shown in in Figs. 1 and 2. Regardless of the dissipation regime (high or low viscosity and resistivity), there is a gap in value of the occupation probabilites; hence, $p_1^{eq} \neq p_2^{eq}$ (two purple curves) and $p_3^{eq} \neq p_4^{eq}$ (two green curves). The physical cause of this gap is the following. The microscopic dynamics is interpreted as the motion of quantum particles moving left and right through a chain of quantum processors. If the likelihood of a quantum particle exiting left or right from a quantum processor is equal, then the excited state energies encoding the left- and right-going probabilities would be degenerate. The equilibrium probabilities must overlap: $p_1^{eq} = p_2^{eq}$ and $p_3^{eq} = p_4^{eq}$. This degeneracy occurs in pairs because there are four occupation probabilities and only two macroscopic field quantities. The macroscopic effective field theory would be strictly diffusive as any quantum particle would move up and down the one dimensional chain of quantum processors in an unbiased random walk fashion. However, if the likelihood of a quantum particle exiting a quantum processor to the left does not equal the likelihood it will exit to the right, then the degeneracy in the distribution functions would be lifted and an energy gap would appear as demonstrated Figs. 1 and 2. In this case, the macroscopic effective field theory would not be strictly diffusive; there would be an overall net advection of quantum particles in one direction (the symmetry of the lattice is broken and this causes an energy gap in excited state energy levels). This net advection gives rise to the nonlinear terms in (2).

The quantum Boltzmann equation is a new modeling tool for numerically predicting the time-dependent behavior of magnetohydrodynamic turbulence and shock formation. Further tests of the algorithm will be presented in a subsequent paper. An open problem is the extending the method to handle magnetohydrodynamic turbulence in two and three spatial dimensions.

REFERENCES

1. J. Yepez, "Lattice-gas quantum computation," *International Journal of Modern Physics C* **9**(8), pp. 1587–1596, 1998. Proceeding of the 7th International Conference on the Discrete Simulation of Fluids, University of Oxford.
2. J. Yepez, "Quantum lattice-gas model for the diffusion equation," *International Journal of Modern Physics C* **12**(9), pp. 1285–1303, 2001.
3. J. Yepez, "Quantum lattice-gas model for the burgers equation," *Journal of Statistical Physics* **107**(1), pp. 203–224, 2002. Presented at the 9th International Conference on Discrete Simulation of Fluid Dynamics, Santa Fe, NM, August 22, 2000.
4. J. Yepez, "An efficient quantum algorithm for the one-dimensional burgers equation," *LANL Archive* , 2002. quant-ph/0210092.
5. L. Vahala, G. Vahala, and J. Yepez, "Lattice boltzmann and quantum lattice representations of one-dimensional magnetohydrodynamic turbulence," *Physics Letters A* **306**, pp. 227–234, 2003.
6. G. Vahala, L. Vahala, and J. Yepez, "Quantum lattice gas representation of some classical solitons," *Physics Letters A* **310**, pp. 187–196, 2003.
7. G. Vahala, L. Vahala, and J. Yepez, "Quantum lattice representation of dark solitons," *SPIE* **5436**, pp. 376–385, 2004.
8. G. Vahala, L. Vahala, and J. Yepez, "Quantum lattice gas representation for vector solitons," *SPIE* **5105**, pp. 187–196, 2003.
9. G. Vahala, L. Vahala, and J. Yepez, "Inelastic vector soliton collisions: a lattice-based quantum representation," *Philosophical Transactions of the Royal Society* **362**(1821), pp. 1677–1690, 2004.
10. J. Yepez, "Type-ii quantum computers," *International Journal of Modern Physics C* **12**(9), pp. 1273–1284, 2001.
11. M. Pravia, Z. Chen, J. Yepez, and D. G. Cory, "Towards an nmr implementation of a quantum lattice gas algorithm," *Computer Physics Communications* **146**(3), pp. 339–344, 2002.
12. M. Pravia, Z. Chen, J. Yepez, and D. G. Cory, "Experimental demonstration of parallel quantum computation," *Quantum Information Processing* **2**, pp. 1–19, 2003.
13. Z. Chen, J. Yepez, and D. G. Cory, "Simulation of the burgers equation by an nmr quantum information processing," *Physical Review A* , Submitted 2004.
14. B. M. Boghosian, J. Yepez, P. Coveney, and A. Wagner, "Entropic lattice boltzmann methods," *Proceedings of the Royal Society of London* **A**(457), p. 717, 2001.
15. B. M. Boghosian, P. Love, P. V. Coveney, I. V. Karlin, S. Succi, and J. Yepez, "Galilean-invariant lattice-boltzmann models with h theorem," *Physical Review E* **68**(025103(R)), 2003.
16. B. Boghosian, P. Love, and J. Yepez, "Entropic lattice boltzmann model for burgers's equation," *Philosophical Transactions of the Royal Society* **362**(1821), pp. 1691–1701, 2004.
17. J. Thomas *Physics of Fluids* **11**, p. 1245, 1968.
18. J. Fleischer and P. Diamond *Physical Review E* **61**, p. 3912, 2000.
19. S. Galtier, "A 1-d mhd model of solar flares: Emergence of a population of weak events, and a possible road toward nanoflares," *The Astrophysical Journal* **521**, pp. 483–489, 1999.
20. W. Woyczynski in *Burgers-KPZ Turbulence: Gottingen Lectures*, **1700**, Lecture Notes in Computer Science, Springer-Verlag, 1998.
21. E. Hopf *Communications on Pure & Applied Mathematics* **3**, p. 201, 1950.
22. J. Cole *Quarterly of Applied Mathematics* **9**, p. 225, 1951.